A selective blocker of Kv1.2 and Kv1.3 potassium channels from the venom of the scorpion *Centruroides suffusus suffusus*☆

Gerardo Corzo [a,1], *Ferenc Papp* [b,1], *Zoltan Varga* [c], *Omar Barraza* [a], *Pavel G. Espino-Solis* [a], *Ricardo C. Rodríguez de la Vega* [a,2], *Rezso Gaspar* [c], *Gyorgy Panyi* [c], *Lourival D. Possani* [a,*]

[a] *Departamento de Medicina Molecular y Bioprocesos, Instituto de Biotecnología, Universidad Nacional Autónoma de México, UNAM. Apartado Postal 510-3, Cuernavaca Morelos 62250, Mexico*
[b] *Cell Biology and Signaling Research Group of the Hungarian Academy of Sciences, Department of Biophysics and Cell Biology, Research Center for Molecular Medicine, University of Debrecen 4012, Hungary*
[c] *Department of Biophysics and Cell Biology, Research Center for Molecular Medicine, University of Debrecen, Medical and Health Science Center, Debrecen 4012, Hungary*

ARTICLE INFO

ABSTRACT

A novel potassium channel blocker peptide was purified from the venom of the scorpion *Centruroides suffusus suffusus* by high-performance liquid chromatography and its amino acid sequence was completed by Edman degradation and mass spectrometry analysis. It contains 38 amino acid residues with a molecular weight of 4000.3 Da, tightly folded by three disulfide bridges. This peptide, named Css20, was shown to block preferentially the currents of the voltage-dependent K+-channels Kv1.2 and Kv1.3. It did not affect several other ion channels tested at 10 nM concentration. Concentration–response curves of Css20 yielded an IC50 of 1.3 and 7.2 nM for Kv1.2- and Kv1.3-channels, respectively. Interestingly, despite the similar affinities for the two channels the association and dissociation rates of the toxin were much slower for Kv1.2, implying that different interactions may be involved in binding to the two channel types; an implication further supported by *in silico* docking analyses. Based on the primary structure of Css20, the systematic nomenclature proposed for this toxin is α-KTx 2.13.

1. Introduction

The venom of scorpions is a valuable source of novel peptides that bind to ion channels and can serve as templates for the design of therapeutic drugs [1]. In case of electrically excitable cells, such as neurons and cardiac muscle cells, it is well accepted that pharmacological interference with plasma membrane ion channels significantly alters the physiological

properties of the cells. Furthermore, block or activation of several voltage-gated ion channels (e.g. block of voltage-gated Na^+-channels by local anesthetics) or ligand-gated channels (e.g. inhibition of nicotinic acetylcholine receptors by muscle relaxants during general anesthesia) was reported to have therapeutic effect.

With the advancement of cellular electrophysiology, especially patch-clamp, the physiological roles of different ion channels were discovered in a variety of cells, including those of voltage-gated Kv1.3 and Ca^{2+}-activated IKCa1 (systematic nomenclature $K_{Ca}3.1$) potassium channels in lymphocytes. Antigen-induced activation and proliferation of lymphocytes were shown to depend indirectly on the activity of these channels [2,3], mainly through the contribution of Kv1.3- and IKCa1-channels to the membrane potential of these cells. A negative membrane potential is required for efficient Ca^{2+} signaling leading to the proliferation of T cells, thus, K^+-channel blockers emerged as potential immunosuppressors [4,5].

Selective and high affinity Kv1.3 inhibitors came into focus upon the discovery of the change in the K^+-channel expression of T cells in parallel with their terminal differentiation [5]. Effector memory T cells (T_{EM}) express dominantly Kv1.3-channels; the level of Kv1.3 expression exceeds several times the ones found in other T cell populations. Accordingly, the membrane potential control and proliferation of T_{EM} is sensitive to Kv1.3 inhibitors whereas other T cells (naïve and central memory T cells) escape Kv1.3 blocker-induced inhibition of proliferation by up-regulating IKCa1 K^+-channels. As T_{EM} cells are responsible for the execution of tissue damage in autoimmune diseases the selective inhibition of Kv1.3-channels is a vital alternative to conventional immunosuppression.

One way of achieving selective Kv1.3 inhibition is to use natural peptide toxins or their derivatives, which bind to the extracellular mouth of K^+-channels (1). Selective binding of the toxins to the channels is not simple, a relatively large number of contacts between toxin and channel residues define the interaction surface. Although the general structure and the folding of K^+-channel blocker scorpion toxins is quite similar, some scorpion toxins of the α-KTx family tend to have a remarkable selectivity among K^+-channels in general and among Shaker-related K^+-channels (Kv1.x) in particular [1], whereas other toxins bind similarly to distantly related channels as well [6]. Identification of key residues influencing binding of α-KTx to each channel is critical for improving the selectivity of a given toxin. This is especially important for therapeutic application of Kv1.3 inhibitors. Noxiustoxin (α-KTx 2.1) for example inhibits Kv1.3 and Kv1.2 with almost identical affinities [1]. Kv1.2-channels are found predominantly in the brain and spinal cord where they play an important physiological role in the control of membrane potential and electrical excitability. Kv1.2 subunits readily associate with other members of the *Shaker* family to form heterotetramer channels [7,8]. These channels are also present in neurons of larger diameter associated with mechanoreception in pain-sensing terminals [9]. Thus, a toxin which inhibits both Kv1.3- and Kv1.2-channels might have significant side effects if applied to a living organism. However, the determination of the molecular interactions of such a toxin with Kv1.3 and Kv1.2 and their comparison to the

ones characteristic for either Kv1.3- or Kv1.2-specific toxins may reveal critical information about structural elements providing selectivity.

One of our research interests has been the identification and purification of naturally occurring biological peptides that affect potassium ion channels in T lymphocytes. Here, we report the primary structure and the pharmacological properties of a potassium ion channel blocker from the venom of the buthid scorpion *Centruroides suffusus suffusus* that blocks voltage-gated Kv1.2- and Kv1.3-channels. *In silico* models of the interactions of Css20 with several Kv ion channels were performed to support our conclusions.

2. Materials and methods

2.1. Materials

Phytohemagglutinin A and other chemicals for electrophysiology were purchased from Sigma–Aldrich Corp. (St. Louis, MO, USA and Budapest, Hungary). Chemicals and HPLC solvents were of analytical grade, described elsewhere [10,11].

2.2. Isolation and chemical characterization of Css20

Scorpions of the species *C. s. suffusus* collected in the field were anesthetized with carbon dioxide and electrically stimulated at the telson (last postabdominal segment), which contains the venomous glands. The crude venom (10 mg) was resuspended in 0.1% aqueous TFA, and the insoluble material was removed by centrifugation at $14,000 \times g$ for 5 min. The supernatant was used directly for HPLC separation. The diluted venom was fractionated using a reverse-phase semipreparative C_{18} column ($5C_{18}MS$, 10 mm × 250 mm Nacalai Tesque Japan) equilibrated in 0.1% TFA, and eluted with a linear gradient of acetonitrile from 0 to 60% in 0.1%TFA, run for 60 min at a flow rate of 2 ml/min as described previously [12]. Effluent absorbance was monitored at 280 nm. Fractions were collected in 1.5 ml plastic tubes and dried out under vacuum. The fractions were subject to electrophysiological assays. Peptide fractions inhibiting Kv1.3-channels (see below) were subjected to a final step of purification performed by a C_{18} reverse-phase column (4.6 mm × 250 mm, Nacalai Tesque, Japan) equilibrated in 0.1% TFA, and eluted with a linear gradient of acetonitrile from 20 to 60% in 0.1%TFA, run for 40 min at a flow rate of 1 ml/min. The pure components were again subjected to electrophysiological assays for detailed pharmacological analysis. The primary structure of the most effective peptide was analyzed by direct sequencing of the native toxin (Edman degradation), using a LF3000 Protein Sequencer (Beckman, CA, USA) and techniques already described by our group [13]. The molecular mass of the pure peptide was confirmed by electro spray ionization mass spectrometry using a Finnigan LCQ^{DUO} ion trap mass spectrometer (San Jose, CA, USA).

2.3. Cells

2.3.1. Lymphocyte separation
Kv1.3 currents were measured in human peripheral T lymphocytes. Heparinized human peripheral venous blood

was obtained from healthy volunteers. Mononuclear cells were separated by Ficoll-Hypaque density gradient centrifugation. Collected cells were washed twice with Ca^{2+} and Mg^{2+} free Hank's solution containing 25 mM HEPES buffer (pH 7.4). Cells were cultured in a 5% CO_2 incubator at 37 °C in 24 well culture plates in RPMI-1640 supplements with 10% FCS (Sigma–Aldrich, Hungary) 100 μg/ml penicillin, 100 μg/ml streptomycin and 2 mM L-glutamine at 0.5×10^6/ml density for 3–4 days. The culture medium also contained 2.5 or 5 μg/ml of phytohemagglutinin A (PHA-P, Sigma–Aldrich Kft, Hungary) to increase K^+-channel expression [14].

2.3.2. Heterologous expression of channels

Cos-7 cells were transiently transfected with the plasmid for hIKCa1 (subcloned into the pEGFP-C1 (Clontech) in frame with green fluorescence protein (GFP), a gift of H. Wulff, UC Davis, CA, USA); or co-transfected with plasmids for GFP and for hKv1.2 (pcDNA3/Hygro vector containing the full coding sequence for Kv1.2, a gift from S. Grissmer, U. of Ulm); or hKv1.4 (hKv1.4ΔN: the inactivation ball deletion mutant of Kv1.4, a gift from D. Fedida, University of British Columbia, Vancouver, Canada); or rKv2.1 (rKv2.1, a gift from S. Korn, U. of Connecticut); or hNav1.5 (a gift from R. Horn, Thomas Jefferson University, Philadelphia, PA, USA). hBK (hSlo1 gene (U11058), in pCI-neo plasmid, a gift from T. Hoshi, University of Pennsylvania, Philadelphia, PA) and hKv1.5 (a gift from D. Fedida, University of British Columbia, Vancouver, Canada) channels were transiently co-transfected into tsA-201 cells along with plasmids encoding GFP.

Transfections were done at a GFP:channel DNA molar ratio of 1:5 using Lipofectamine 2000 reagent according to the manufacturer's protocol (Invitrogen, Carlsbad, CA, USA), and cultured under standard conditions. Currents were recorded 1 day after transfection. GFP positive transfectants were identified in a Nikon TE2000U fluorescence microscope. More than 70% of the GFP positive cells expressed the co-transfected ion channels.

Cos-7 cells were maintained in standard cell culturing conditions [13]. Human embryonic kidney cells transformed with SV40 large T antigen (tsA201) were grown in Dulbecco's minimum essential medium–high glucose supplemented with 10% FBS, 2 mM L-glutamine, 100 U/ml penicillin-G, and 100 μg/ml streptomycin (Invitrogen) at 37 °C in a 9% CO_2 and 95% air-humidified atmosphere. Cells were passaged twice per week after 7-min incubation in Versene containing 0.2 g/L EDTA (Invitrogen).

hERG channels were expressed in a stable manner in a HEK-293 cell line. L929 cells stably expressing mKv1.1-channels have been described earlier [15] and were gifts of H. Wulff (UC Davis, CA, USA).

2.4. Electrophysiology

Whole-cell currents were measured in voltage-clamped cells using Axopatch 200A and Multiclamp 700B amplifiers connected to a personal computer using Axon Digidata 1200 and 1322A data acquisition hardware, respectively (Molecular Devices Inc., Sunnyvale, CA). Series resistance compensation up to 70% was used to minimize voltage errors and achieve good voltage-clamp conditions. Cells were observed with

Nikon TE2000-U or Leitz Fluovert fluorescence microscopes using bandpass filters of 455–495 nm and 515–555 nm for excitation and emission, respectively. Cells displaying strong fluorescence were selected for current recording and >70% of these cells displayed co-transfected current. Pipettes were pulled from GC 150 F-15 borosilicate glass capillaries in five stages and fire-polished, resulting in electrodes having 3–5 MΩ resistance in the bath. For the measurement of most channels the bath solution consisted of (in mM) 145 NaCl, 5 KCl, 1 $MgCl_2$, 2.5 $CaCl_2$, 5.5 glucose, and 10 HEPES, pH 7.35, supplemented with 0.1 mg/ml bovine serum albumin (Sigma–Aldrich). For the recording of hERG currents the bath solution contained (in mM): 140 Choline-Cl, 5 KCl, 2 $MgCl_2$, 2 $CaCl_2$, 0.1 $CdCl_2$, 20 glucose, and 10 HEPES, pH 7.35. The measured osmolarity of the external solutions was between 302 and 308 mOsm. The internal solution consisted of (in mM): 140 KF, 2 $MgCl_2$, 1 $CaCl_2$, 10 HEPES, and 11 EGTA, pH 7.22. For the recording of hBK currents the composition of the pipette filling solution was (in mM): 140 KCl, 10 EGTA, 9.69 $CaCl_2$, 5 HEPES (pH 7.2). The free Ca^{2+} concentration of this latter solution is $[Ca^{2+}]_{int} = 5$ μM, which allows the recording of BK currents at moderate depolarizing potentials [16]. For the recording of hIKCa1 currents the composition of the pipette filling solution was (in mM): 150 K-aspartate, 5 HEPES, 10 EGTA, 8.7 $CaCl_2$, 2 $MgCl_2$, (pH 7.2). This solution contained 1 μM free Ca^{2+} concentration to fully activate the hIKCa1 current. For the recording of hERG currents the pipette solution contained (in mM): 140 KCl, 10 EGTA, 2 $MgCl_2$, 10 HEPES (pH 7.3). The measured osmolarity of the internal solutions was approximately 295 mOsm. Bath perfusion around the measured cell with different test solutions was achieved using a gravity-flow perfusion system. Excess fluid was removed continuously. For data acquisition and analysis, the pClamp8/10 software package (Molecular Devices Inc., Sunnyvale, CA) was used. Generally, currents were low-pass filtered using the built in analog 4-pole Bessel filters of the amplifiers and sampled (2–50 kHz) at least twice the filter cut-off frequency. Specific details about filter setting data acquisition rate combinations are in the figure legends. Before analysis, whole-cell current traces were corrected for ohmic leakage and digitally filtered (three-point boxcar smoothing). Each data point on the concentration–response curve represents the mean of three to seven independent experiments, and error bars represent S.E.M. Data points were fitted with a two parameter Hill-equation: $RCF = K_d^n/(K_d^n + [Tx]^n)$, where RCF is the remaining current fraction ($RCF = I/I_0$, where I and I_0 are the current amplitudes in the presence and absence of the toxin of given concentration, respectively), K_d is the dissociation constant, n is the Hill coefficient and [Tx] is the toxin concentration.

2.5. Molecular modeling

The sequence of Css20 was compared against PDB [17] with BLAST protocol [18], aiming to identify the most suitable structure for homology modeling. The structure of α-KTx 2.2 (Margatoxin, PDB code 1mtx) was used as a template due to a high amino acid sequence identity and similar pharmacological profile. Fifty models were calculated in the program Modeller 9v2 [19], and the five models with the lowest energy were used for rigid docking as described below. To generate a

model of the hKv1.2-channel, the missing side chains in the structure of rKv1.2 (PDB code 2a79) were modeled in the PDB_Hydro web server (lorentz.immstr.pasteur.fr/pdb_hy-dro.php [20]). A D355E substitution within the rKv1.2-channel outer mouth was introduced with Modeller 9v2. The tetrameric structure was formed by superposition of pore lining segments over each monomer of the KcsA-channel (PDB code 1bl8), with further refinement in Modeller 9v2. The models of hKv1.1, hKv1.3 and hKv1.4 were calculated using the same program, with the model of hKv1.2 as template. The lowest energy models of 25 calculations for each channel were energetically optimized and used for the rigid docking.

The structures of the complexes between Css20 and each channel were modeled with the program ZDOCK 2.3 [21], which executes a fast Fourier transform search of all possible binding modes; evaluated on the basis of shape complementarities, electrostatic and desolvation energies. For every of the five final Css20 models, 54,000 complexes were calculated with each channel (5 Css20 models $\times$ 54,000 dockings $\times$ 4 channels = 1,080,000 complexes). These complexes were then ranked with ZRANK [22] and the one hundred best ranking complexes of every set (i.e. 5 Css20 model $\times$ 4 channels $\times$ 100 dockings = 2000 complexes in four sets) were visually inspected. From these, the best 10 models in which the toxin binds with a critical residue (K28) to the ion channel's selectivity filter (see below) were minimized with Chimera [23], under Amber force field, taking into consideration the zone of interaction (the whole toxin and the ion channel's extracellular mouth). When needed, further minimizations were performed with the same program but keeping the channel rigid. Finally, the 10 selected models from each set were further refined with FireDock [24] and the results analyzed in the PISA web server (www.ebi.ac.uk/msd-srv/prot_int/cgi-bin/piserver [25]) in order to calculate average interface area, desolvation free energy gain and the relative interfaces' hydrophobicity. R.M.S.D.s were calculated with MolMol [26]. Hydrogen bonds were identified with LIGPLOT 4.4.2 [27] and PISA web server. Models were displayed with PyMol (www.pymol.org).

3. Results

3.1. Purification and amino acid sequence determination

The soluble venom of C. s. suffusus was fractionated using reverse-phase HPLC (Fig. 1). Fractions were manually collected and vacuum-dried. Each fraction was separately resuspended in the appropriate bath solution and their affinity for Kv1.3-channels in human lymphocytes was assayed under voltage-clamp conditions. Only fraction 20 (Fig. 1) blocked Kv1.3 currents of lymphocytes at the concentration assayed (0.7 μg/ml, data not shown). This fraction was further separated by reverse-phase HPLC chromatography under different conditions (see Fig. 2), in order to obtain a homogeneous peptide. The highly purified peptide showed qualitatively similar Kv1.3 blocking properties as observed previously with the whole fraction 20. The pure peptide was alkylated and sequenced by Edman degradation. The alkylated toxin gave unequivocal amino acid sequence up to residue at position 37 (Table 1). The
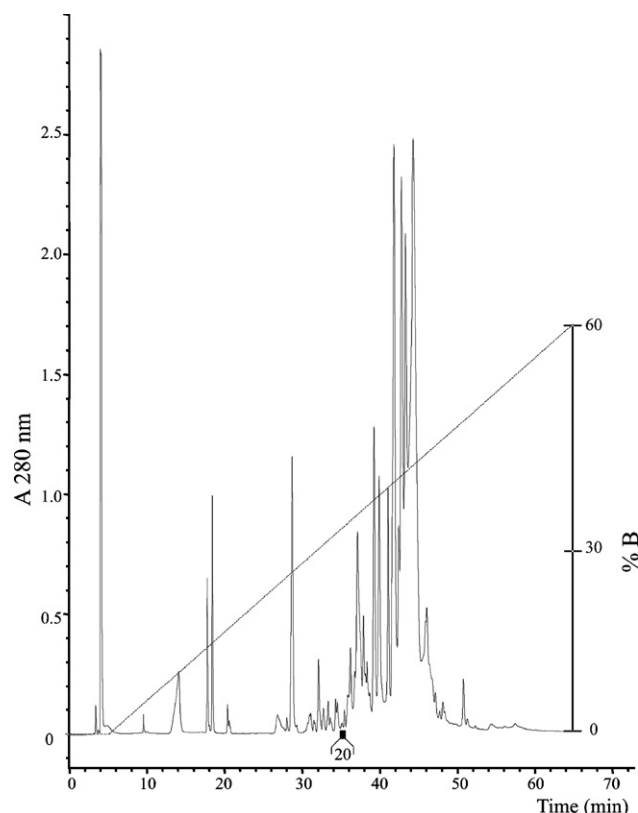

Fig. 1 – Reverse-phase HPLC chromatogram of the venom of C. s. suffusus. The soluble venom of C. s. suffusus (obtained from 10 mg crude whole venom, see Section 2) was fractionated using a reverse-phase semipreparative C_{18} column ($5C_{18}MS$, 10 mm $\times$ 250 mm) equilibrated in 0.1% TFA, and eluted with a linear gradient of acetonitrile from 0 to 60% in 0.1%TFA, run for 60 min at a flow rate of 2 ml/min. The small peak indicated by number 20 in the figure was the fraction that gave positive results in blocking Kv1.3 at 10 nM concentration, and was further purified to homogeneity.

full-length toxin and the C-terminal proline residue were confirmed and identified by mass spectrometry. The peptide contains 38 amino acid residues with an experimentally determined molecular mass of 4000.3 atomic mass units. The theoretical expected molecular mass was 4000.8, confirming the full amino acid sequence. In its native conformation the six cysteines form three disulfide bridges. Css20 shares over 54% identity with other toxic peptide blockers of voltage-gated potassium channels, belonging to the α-KTx2 subfamily isolated from buthid scorpions, as shown in Table 1. The closest similar toxin (81%) is CllTx1 (α-KTx 2.3) purified from the Mexican scorpion Centruroides limpidus limpidus. Among other similar peptides are: Noxiustoxin (P08815, α-KTx 2.1), Margatoxin (P40755, α-KTx 2.2) and Hongotoxin-1 (P59847, α-KTx 2.5). Considering the amino acid sequence similarities with the toxins listed in Table 1, and the criteria defined by Tytgat and coworkers [28], the proposed systematic name of Css20 is α-KTx 2.13. Like other members of this subfamily, α-KTx 2.13 is a basic peptide with an isoelectric point (pI) of 9.2 (Table 1). Although this peptide fits into the large list of
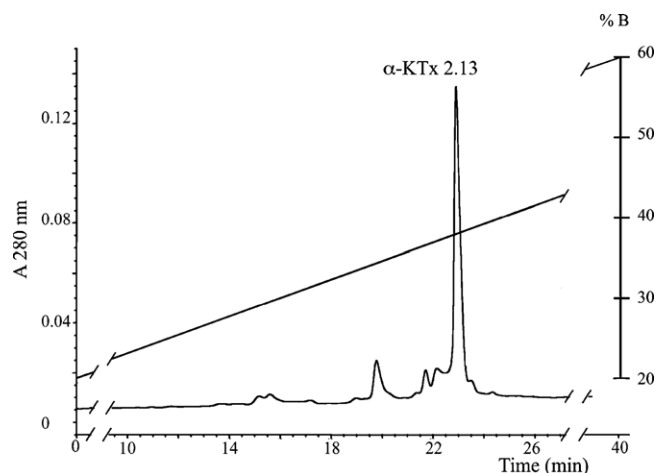
Fig. 2 – Reverse-phase HPLC chromatogram of the fraction Css20. A sample containing 12 μg of component 20 from the previous column was finally separated by HPLC, using a C$_{18}$ column (5C$_{18}$MS, 4.6 mm × 250 mm) equilibrated in 0.1% TFA, and eluted with a linear gradient of acetonitrile from 20 to 60% in 0.1%TFA, run for 40 min at a flow rate of 1 ml/min. The pure peptide α-KTX2.13 was the only fraction that gave positive results in blocking Kv1.3. It corresponds to only about 0.1% of the soluble venom.

existing toxic peptides that affect K$^+$-channels, the most relevant contribution of this communication resides on the electrophysiological findings described below and on the molecular modeling, where original findings are described.

3.2. Pharmacological properties of Css20

The effect of Css20 was tested on a variety of ion channels using the patch-clamp technique. Fig. 3 shows that the toxin blocks potassium currents through Kv1.2- and Kv1.3-channels

in the nanomolar concentration range. Fig. 3(A) displays macroscopic K$^+$ currents through Kv1.2-channels recorded sequentially in the same cell, before (control) and after the addition of 3 nM Css20 to the external solution. Kv1.2 currents were measured in whole-cell voltage-clamped Cos-7 cells (for experimental conditions see Section 2 and the figure legend). The displayed record in the presence of Css20 was taken after the equilibration of the block. Under these conditions approximately 75% of the Kv1.2-channels were blocked. The block was partially reversed by perfusing the cell with toxin-free external solution (wash-out, the trace shown was recorded 13 min after the removal of the toxin). The kinetics of both toxin association and dissociation were slow, several minutes were required to reach steady-state block and many minutes of wash-out with toxin-free solution resulted in an incomplete recovery from block (Fig. 3(B)).

As Fig. 3(C) demonstrates Css20 was less effective on Kv1.3-channels. Under the experimental conditions applied to human peripheral blood T cells (detailed in Section 2 and in the figure legend) the whole-cell currents recorded were conducted exclusively by the endogenously expressed Kv1.3-channels [33]. Extracellular application of 10 nM Css20 reduced the whole-cell K$^+$ current by approximately 60%. The block of Kv1.3-channels by the toxin was fully reversible and had very fast kinetics. Both the equilibration of the block and full relief from the block took place between two subsequent depolarizing pulses separated by 30 s (Fig. 3(D)).

The concentration–response functions of Css20 on both Kv1.2- and Kv1.3-channels were constructed by determining the remaining fraction of the whole-cell current in the presence of various concentrations of the toxin (Fig. 4). The remaining current fractions (RCF) were calculated as I/I_0 where I_0 and I are the peak K$^+$ currents measured in control solution and after equilibrium block of the current in the presence of the toxin at the indicated concentrations, respectively. The concentration–response curve was fit with a Hill equation (see legend) with the only two free parameters being the

Family	Name	Peptide					pI	Identity (%)	Kv1.2 K$_d$ (nM)	Kv1.3 K$_d$ (nM)	Accession number
		1	10	20	30	39					
α-KTx 2.1	Noxiustoxin	TIINVK**C**TSPKQ**C**SKP**C**KELYGSSAGAK**C**MNGK**C**K**C**Y**NN**					9.2	68	2[a]	1[a]	P08815
α-KTx 2.2	Margatoxin	TIINVK**C**TSPKQ**C**LPP**C**KAQFGQSAGAK**C**MNGK**C**K**C**Y**PH**					9.2	76	0.6[b] >30[c]	0.23[b] 0.05[d]	P40755
α-KTx 2.3	ClITx1 (II.10.9.1)	ITINVK**C**TSPQQ**C**LRP**C**KDRFGQHAGG**K****C**INGK**C**K**C**YP					9.3	81	ND	ND	P45629
α-KTx 2.4	Cn Ntx2	TIINEK**C**FATSQ**C**WTP**C**KKAIG–SLQSK**C**MNGK**C**K**C**YNG					9.0	55	ND	ND	Q9TXD1
α-KTx 2.5	Hongotoxin-1	TVIDVK**C**TSPKQ**C**LPP**C**KAQFGIRAGAK**C**MNGK**C**K**C**Y**PH**					9.2	73	0.17[b]	0.09[b]	P59847
α-KTx 2.6	Hongotoxin-3	TFINVK**C**TSPKQ**C**LPA**C**KEKFGXAAG–K**C**MNGK**C**K?					9.4	70	ND	ND	[29]
α-KTx 2.7	ClITx2 (II.9.2)	TVIDVK**C**TSPKQ**C**LPP**C**KEIYGRHAGA**C**MNGK**C**K**C**					9.0	63	ND	ND	P45630
α-KTx 2.8	Ce1 toxin	TVINVK**C**TSPKQ**C**LKP**C**KDLYGPHAGAK**C**MNGK**C**K**C**YNN					9.2	67	ND	0.71[d]	P0C161
α-KTx 2.9	Ce2 toxin	TIINVK**C**TSPKQ**C**LKP**C**KDLYGPHAGAK**C**MNGK**C**K**C**YNN					9.2	64	ND	0.25[d]	P0C162
α-KTx 2.11	Ce4 toxin	TIINVK**C**TSPKQ**C**LLP**C**KEIYGIHAGAK**C**MNGK**C**K**C**YKI					9.2	54	ND	0.98[d]	P0C164
α-KTx 2.13	Css20-3	IFINVK**C**SSPQQ**C**LKP**C**KAAFGISAGG**K****C**INGK**C**K**C**YP					9.2	100	1.3	7.2	P85529

ND, not determined.
[a] rKv1.2- and mKv1.3-channels expressed in B82 mouse fibroblast and L929 cells, respectively [15].
[b] Kv1.2- and Kv1.3-channels expressed in HEK-293 cells [29].
[c] Kv1.2-channels in striatal medium spiny neurons [30].
[d] Kv1.3-channels expressed in human lymphocytes [31,32].

Table 1 – Sequence alignment and dissociation constants of members of the α-KTx 2 subfamily for Kv1.2 and Kv1.3
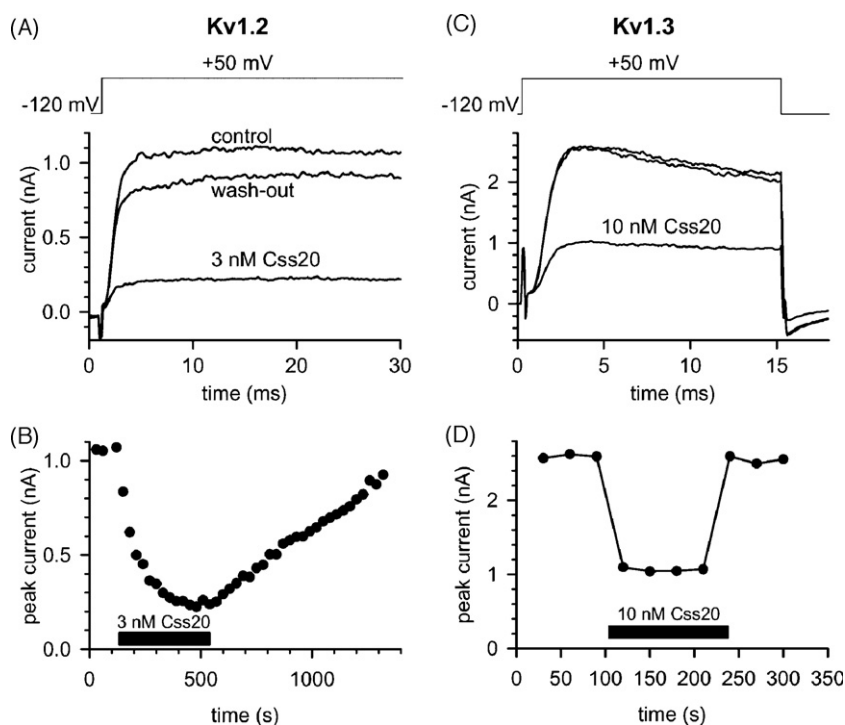
Fig. 3 – Css20 reversibly blocks Kv1.2- and Kv1.3-channels with high affinity. (A) K$^+$ currents of a Cos-7 cell expressing hKv1.2-channels were recorded in whole-cell configuration during 200-ms-long test pulses to +50 mV from a holding potential of −120 mV (voltage protocol is shown above the current records, shorter segments of the full records are shown for easier comparison of the peaks). Test pulses were applied every 30 s. The bath was perfused continuously. Representative traces show the K$^+$ current before the application of the toxin (control), after the equilibration of the block in the presence of 3 nM Css20 (as indicated) and after partial recovery from block during the perfusion of the bath with toxin-free solution (wash-out). Sampling frequency: 10 kHz, analog low pass filter: 5 kHz, digital boxcar filter: 3 points. (B) Time course of the development and the removal of K$^+$ current block for the cell shown in panel (A). Peak K$^+$ currents were determined and plotted as a function of time. The bar above the time axis indicates the period of the application of 3 nM Css20. (C) K$^+$ currents of a human T lymphocyte endogenously expressing Kv1.3-channels were recorded in whole-cell configuration during 15-ms-long test pulses to +50 mV from a holding potential of −120 mV (see the voltage protocol above the currents). Test pulses were applied every 30 s. Sampling frequency: 20 kHz, analog low pass filter: 5 kHz, digital boxcar filter: 3 points. Other experimental conditions were the same as for panels (A) and (B). (D) Time course of the development and the removal of K$^+$ current block for the cell shown in panel (C).

dissociation constant (K_d) and the Hill coefficient (n). The resulting K_d values and Hill coefficients were K_d = 1.26 nM, n = 1.17 for Kv1.2 and K_d = 7.21 nM, n = 0.90 for Kv1.3. The values of the Hill coefficient indicate that the interaction of the Css20 peptide with the potassium channel pore follows the general blocking scheme of pore blocking toxins: one peptide binds per channel [34].

We have tested the effect of Css20 on other ion channels expressed by various cell lines (see Section 2 and the figure legend). These included three members of the voltage-gated *Shaker* family, Kv1.1, Kv1.4 and Kv1.5, most closely related to the channels blocked by the toxin. In addition, Kv2.1, a member of the *Shab* family, hERG (Kv11.1), a voltage-gated cardiac K$^+$-channel, IKCa1 (K$_{Ca}$3.1), an intermediate conductance Ca^{2+}-activated potassium channel also expressed by lymphocytes, BKCa (K$_{Ca}$1.1), a big conductance voltage and Ca^{2+}-activated potassium channel and Nav1.5, a cardiac sodium channel were also tested. As shown by Fig. 5(A–H), none of the tested ion channels were significantly affected by

the toxin, except for Kv1.2 and Kv1.3 described above. The application of 10 nM Css20 reduced Kv1.2 currents by 93%, Kv1.3 currents by 58%, whereas the reduction of the currents through other channels was less than 7%. This means an estimated $K_d > 150$ nM for Kv2.1, the third most affected channel, and even much greater values for the other channels. Thus, Css20 is selective for Kv1.2 and Kv1.3 over the other ion channels examined in this study (Fig. 5(I)).

3.3. Molecular modeling

Taking advantage of the well-defined interaction mode between α-KTx peptide inhibitors and Kv channels [35,36], molecular models of Css20 interacting with hKv1.1, 1.2, 1.3 and 1.4 channels were obtained as described in Section 2. Five Css20 models, with an average side chain R.M.S.D. of 1.35 ± 0.14 Å, were docked into each of the four channel constructs with ZDOCK (it is worth mentioning that rigid body docking performance is usually increased if multiple initial
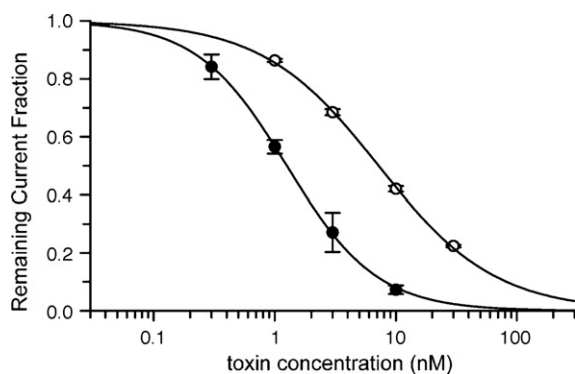
Fig. 4 – Concentration dependence of K$^+$ current block by Css20. The remaining fraction of the Kv1.2 (filled circles) or Kv1.3 (empty circles) current (RCF) was calculated as I/I_0, where I_0 and I are the peak K$^+$ currents measured in the control solution and during bath perfusion with the test solution containing the toxin at indicated concentrations, respectively. The voltage protocol and other experimental conditions were the same as in Fig. 3. The superimposed solid line is the binding curve fitted to the data points: $RCF = K_d^n/(K_d^n + [Tx]^n)$, where [Tx] indicates the toxin concentration, K_d is the dissociation constant and n is the Hill coefficient. The best fit yielded $K_d = 1.26$ nM, $n = 1.17$ for Kv1.2 and $K_d = 7.21$ nM, $n = 0.90$ for Kv1.3. Error bars indicate S.E.M. ($n = 3$–7).

conformations could mimic side chain flexibility [37,38]). PISA analysis of the 10 selected models for each interacting pair – after FireDock refinement – suggests that Css20 fits well on the outer mouth of hKv1.2 and hKv1.3, but not so well on hKv1.1 or hKv1.4 (see Table 2). To discriminate between Css20 interacting with these channels, we used a FireDock-based scoring function [24], taking into consideration two more terms referring to the prevalence of the ''principal mode'' over the 100 best solutions of each pair (additive term) and the R.M.S.D. of the channel-bound toxin (subtractive term). These results are in agreement with the pharmacological profile observed in the electrophysiological experiments. Table 2 summarizes the prevalence of the principal mode (see below) amongst the best ranking models, average interface area, desolvation energy, interface's relative hydrophobicity, R.M.S.D. of channel-bound toxin and the average number of contacts.

Further inspection of the selected complexes between Css20 and hKv1.2 and hKv1.3 reveals that almost all of the channels' interacting residues rely on three regions, namely: the outer end of the selectivity filter; the linker between S5 and pore helix (the ''turret''), and the bottom of the channels' vestibule. Seven out of eight amino acid residue differences between the outer mouths of hKv1.2 and hKv1.3 are located in the last two regions. Although there are no evident differences between most of the parameters shown in Table 2, a more detailed analysis of the interaction mode suggests some features which could be related with the different association and dissociation rates of Css20 on both affected channels (see below). Fig. 6 shows one representative complex of Css20 with each channel, hKv1.2 and hKv1.3, highlighting the interacting pairs identified by PISA and LIGPLOT analyses. The distinct

contribution of the amino acid residues situated in the turret region related to the overall contacts for each complex is worth mentioning, with almost twice as many contacts with hKv1.2 than with hKv1.3.

4. Discussion

Toxins purified from the venom of various species that are highly specific blockers of the Kv1.3 potassium channel have gained much interest in recent years due to the prospect of achieving selective immunosuppression by inhibiting the proliferation of certain lymphocyte subsets [5]. To date no such well defined pharmacological target is known for high affinity blockers of the Kv1.2-channel, since this subtype is widespread in the central nervous system and forms heterotetramer channels with other members of the *Shaker* family that are likely to have different pharmacological properties from the homotetrameric channels [7,39]. Thus, a toxin with similar affinities for these two channels, such as Css20, is not an ideal candidate as a potential therapeutic drug. However, there are substantial differences between the inhibitory potencies of Css20 on Kv1.2 and Kv1.3, compared to Kv1.1 and Kv1.4 (well over 100-fold). These 4 channels are closely related with only 9 non-conserved positions over 38 residues which define the interacting surface. Moreover, the blocking kinetics of Kv1.2 (slow) and Kv1.3 (fast) are also significantly different; therefore structure–function studies with such toxins can pinpoint critical residues on channel surfaces and in toxins that determine the affinity of binding and selectivity of toxins for Kv1.2- or Kv1.3-channels. This information then can aid the design of toxins more selective for a particular channel type. Additionally, the analysis reported here opens the field for experiments aiming at expressing specific Css20 mutants, in order to obtain more selective variants of this toxin, with possible preference for one versus the other channels modeled here.

Comparison of the primary sequence of the members of the α-KTx 2 subfamily reveals several highly conserved residues, such as I3, K6, Q12, P16, K18, G22, N31, G32, K33, K28, K35, and Y37 (Table 1). Two of these residues, a critically positioned lysine (K28 in Css20) and an aromatic residue 9 positions downstream (Y37 in Css20), have been referred to as the ''functional dyad'' (the two dyad residues connected in Table 3) because this pair is found in many high affinity K$^+$-channel blocking scorpion toxins, not only in members of the α-KTx 2 subfamily [29,35,40,41]. The ''functional dyad'' seems to be critical for the high affinity block of Kv1.2. Mutation of the dyad residues to alanines reduced the affinity of the toxin Pi1 (α-KTx 6.1) for Kv1.2 by several orders of magnitude [42] and the two corresponding residues in maurotoxin (MTX (α-KTx 6.2), K23 and Y32) also proved essential for high affinity binding to Kv1.2 [43]. The requirement for the dyad is not as straightforward for blocking Kv1.3. Despite the presence of the dyad MTX blocks hKv1.3 very poorly, but the H399T mutation at the bottom of the outer vestibule renders it as sensitive to MTX block as Kv1.2 is. The dyad residue Y32 of MTX was found to interact with residue T399 of mutant hKv1.3, so the interaction between H399 in wild type Kv1.3 and the dyad tyrosine in the toxin seems to interfere with the binding. This
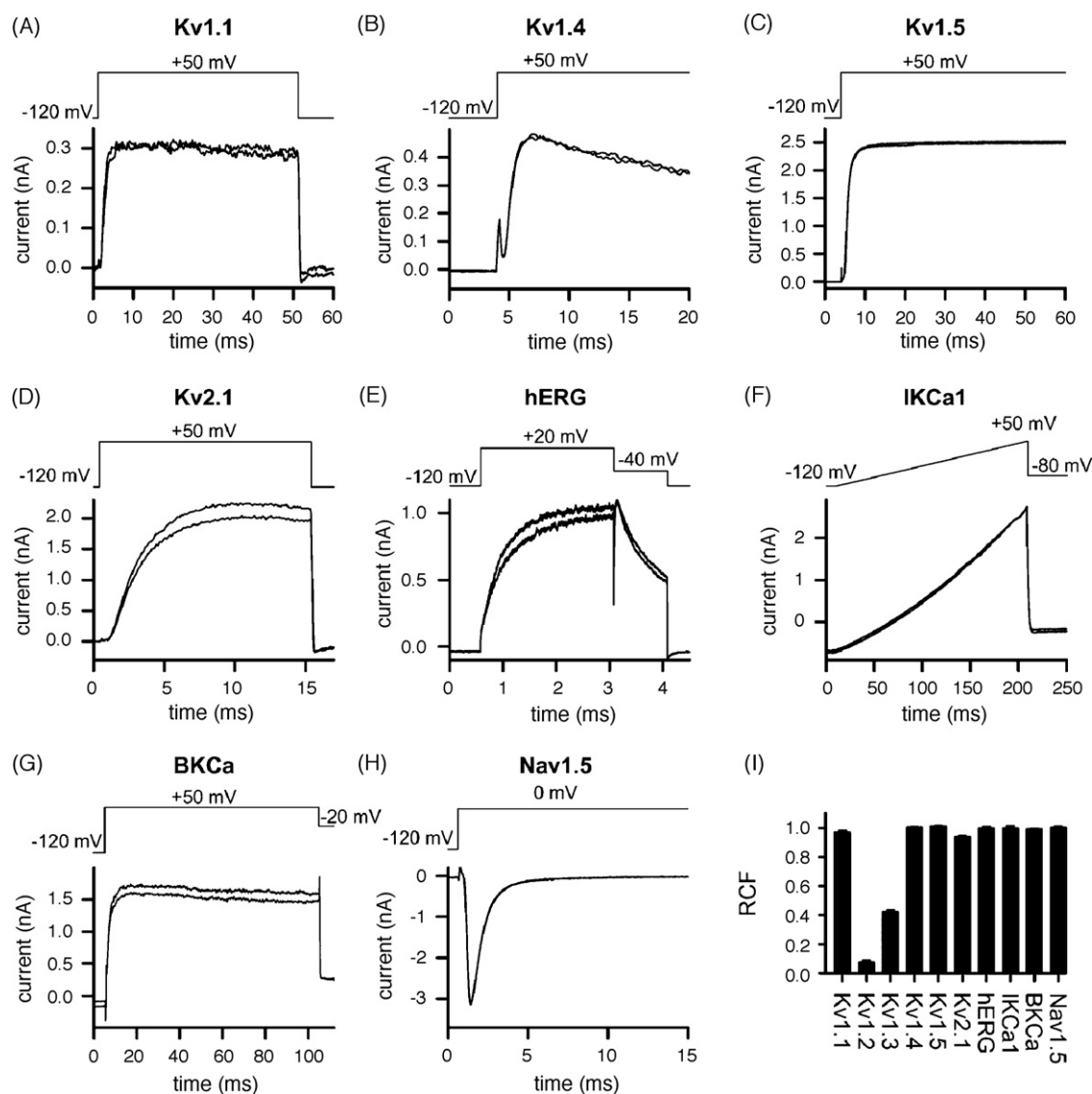
Fig. 5 – Selectivity profile of Css20. The blocking effect of Css20 was assayed on nine potassium channels and a cardiac sodium channel. The channels were expressed as described in Section 2. Representative traces in the absence and in the presence of 10 nM Css20 are shown for each tested channel in panels (A–H), except for Kv1.2 and Kv1.3, which are shown in Fig. 4. In the case of non-overlapping traces the current trace of lower amplitude was recorded in the presence of the toxin. Voltage protocols are shown above the current records. (A–D) Currents through Kv1.1, Kv1.4, Kv1.5 and Kv2.1 were evoked by voltage steps to +50 mV from a holding potential of −120 mV every 15 s. Sampling frequency: 10 kHz, analog low pass filter: 5 kHz, digital boxcar filter: 3 points. The duration of the depolarizing pulses was 200 ms for recording Kv1.4 and Kv1.5 currents. For these latter currents shorter sections of the full records are shown for easier comparison of the peaks. (E) hERG currents were evoked by a voltage step to +20 mV (duration: 2.5 s) followed by a step to −40 mV (duration: 1 s) during which the peak current was measured. The holding potential was −80 mV, pulses were delivered every 30 s. Sampling frequency: 2 kHz, analog low pass filter: 1 kHz, digital boxcar filter: 3 points. (F) IKCa1 (K_{Ca}3.1) currents were evoked by voltage ramps running from −120 to +50 mV every 10 s from a holding potential of −120 mV. Sampling frequency: 10 kHz, analog low pass filter: 5 kHz, digital boxcar filter: 3 points. (G) BK (K_{Ca}1.1) currents were evoked by a voltage step to +50 mV (duration: 100 ms) preceded by a 10-ms hyperpolarization to −120 mV from a holding potential of 0 mV. Pulses were delivered every 5 s. Sampling frequency: 20 kHz, analog low pass filter: 4 kHz, digital boxcar filter: 3 points. (H) Na_V1.5 currents were evoked by voltage steps to 0 mV from a holding potential of −120 mV every 15 s. The duration of the depolarizing pulses was 40 ms; 15-ms-long sections of the full records are shown for easier comparison of the peaks. Sampling frequency: 50 kHz, analog low pass filter: 5 kHz, digital boxcar filter: 3 points. (I) The remaining fraction of the whole-cell current was determined in the presence of 10 nM toxin for each channel. Except for Kv1.2 and Kv1.3 the toxin did not significantly block any of the tested channels.
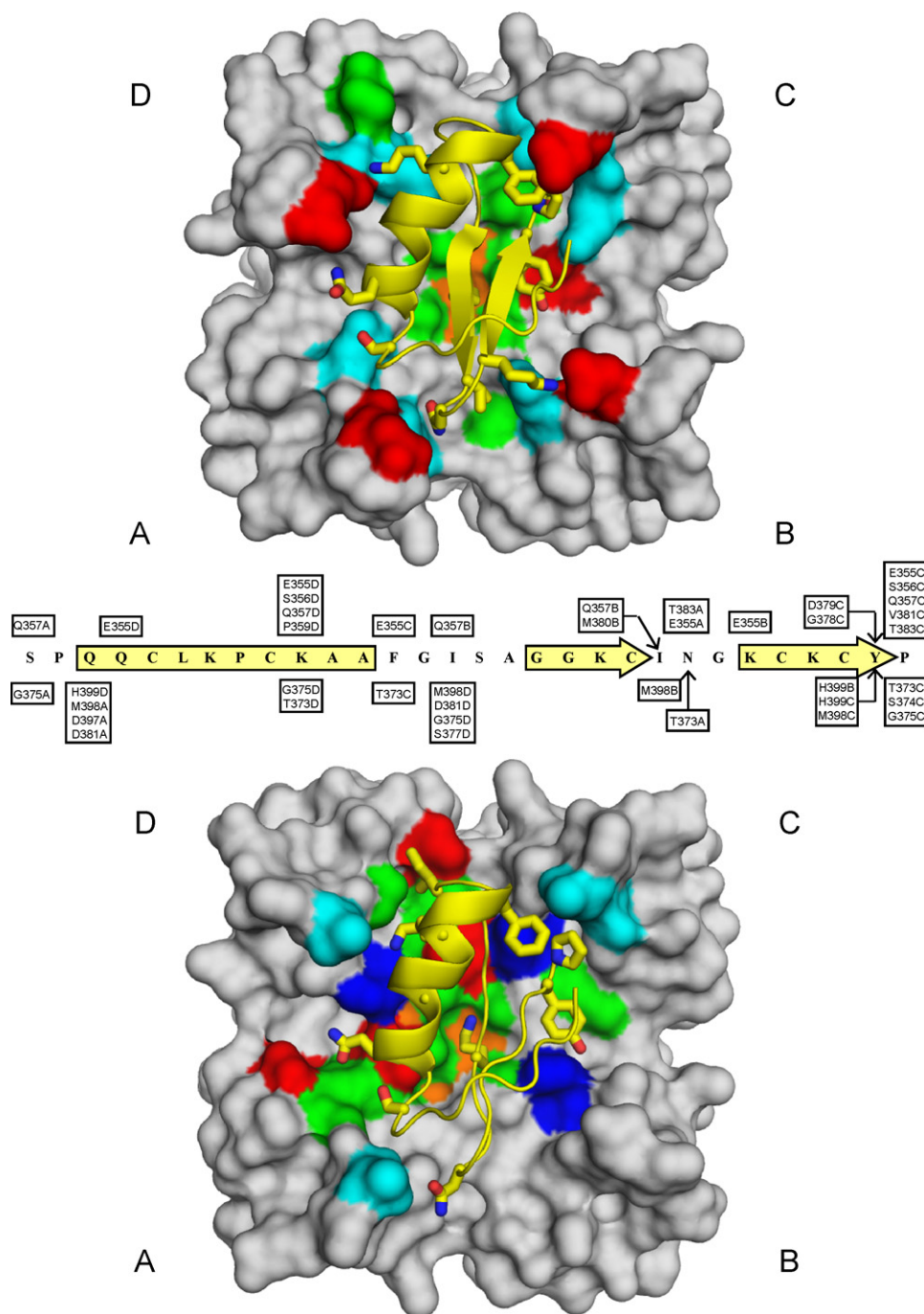
Fig. 6 – Models of the interaction between Css20 and hKv1.2 and hKv1.3. Two representative models of Css20 docked onto hKv1.2 (up) and hKv1.3 (down). Toxin is displayed as yellow cartoons of secondary structure elements and ion channels as molecular surfaces. Side chains of the toxin residues which make contacts with the channels are displayed as sticks with N and O atoms colored blue and red, respectively. Residues of the channels making direct interaction with the toxin are colored as follows: acidic (Asp and Glu), red; basic (Arg, His and Lys), blue; polar (Asn, Gln, Ser and Thr), cyan; hydrophobic (Gly, Met, Pro and Val), green and; aromatic (Tyr), orange. Both figures are displayed in the same orientation. Notice the preponderance of turret residues in the interaction of the toxin with hKv1.2, whereas toxin binding on hKv1.3 is governed mainly through residues at the vestibule and selectivity filter. The middle panel shows the amino acid sequence of the toxin starting with residue number 9 (S9), because no significant interactions exist with either of the channels with residues at the most N-terminal segment of Css20. The amino acids that make contacts with Css20 in hKv1.2 are shown above the toxin sequence, whereas those in hKv1.3 are shown below. The last letters after the residue number of the ion channel subunits, refer to the (A–D) subunits of the tetrameric channel. Subunits are labeled counter-clockwise from (A) to (D) starting from bottom left. For instance, S9 of the toxin makes contact with Q357 at the subunit (A) of the hKv1.2. Interacting pairs were identified as a consensus between PISA and LIGPLOT analyses. Note that residue K28 of the toxin

Table 2 – Molecular modeling parameters

	hKv1.1	hKv1.2	hKv1.3	hKv1.4
Principal mode prevalence[a]	8.3	5.7	10	5.2
Interface area (Å²)[b,c]	1197 ± 124	1238 ± 45	1211 ± 41	1116 ± 61
Desolvation energy[b,c] (kcal/mol)[b]	−6.1 ± 3.3	−10.3 ± 1.6	−11.6 ± 2.6	−9.6 ± 1.9
P-value[b,c]	0.84 ± 0.06	0.76 ± 0.06	0.76 ± 0.08	0.77 ± 0.06
R.M.S.D. (Å) bb/sc[d]	2.1/2.5	1.6/2.1	0.8/1.5	6.7/7.1
Contacts[b]				
Channel[e]	n.c.	7.5 ± 1.6	8.6 ± 2.0	n.c.
Toxin[e]	n.c.	5.6 ± 1.7	6.4 ± 1.3	n.c

Abbreviations: bb, backbone; sc, side chain; n.c., not calculated.
[a] Percentage of principal mode over 100 best scoring ZRANK analysis [21,22].
[b] Average of the 10 top ZRANK scored complexes [22], further refined with FireDock [24].
[c] According to PISA analysis [25].
[d] Calculated "as is" with MolMol [26].
[e] Number of residues involved in direct contacts, as identified by LIGPLOT [27].

must be the case for Css20 as well, as our docking simulations indicate interactions between Y37 of the toxin and H399 on two subunits of hKv1.3. Although there are several toxins bearing a tyrosine at the aromatic dyad position, which block Kv1.3 in the nanomolar range, such as noxiustoxin, hongotoxin-1 and Css20, the selectivity for Kv1.3 seems to benefit from the replacement of this tyrosine by other residues. The most effective scorpion toxin blockers of Kv1.3 have a residue at the "aromatic dyad position" different from tyrosine such as phenylalanine (Pi2, Pi3, anuroctoxin; α-KTx 7.1, 7.2 and 6.12, respectively), threonine (kaliotoxin, OSK1; α-KTx 3.1 and 3.7, respectively) or asparagine (HsTx1 α-KTx 6.3), whereas toxins favoring Kv1.2 over Kv1.3 all have a tyrosine at this position [MTX, Pi1, CoTX1 (α-KTx 10.1), Pi4 (α-KTx 6.4), see Table 3]. Thus, while the critical lysine protruding into the channel pore seems essential for the block of both channels, the tyrosine embodying the other half of the dyad apparently steers selectivity toward Kv1.2. In agreement with this, docking results predict several contacts between the residues Y37 and P38 of the toxin and various residues of both channels (Fig. 6). This suggests that steric constraints at the "aromatic dyad residue" position are very important determinants of high affinity binding.

The significance of the different toxin regions in channel recognition was demonstrated using a chimeric toxin constructed from the α-helical N-terminal region of the Kv1.2-specific MTX and the C-terminal region of the Kv1.3-specific HsTx1 (the two regions separated by the dashed line in Table 3). The study showed that the replacement of the C-terminal half of MTX, which includes the β-hairpin region, with that of HsTx1 completely abolished high affinity block of Kv1.2 indicating the relevance of this segment in the selectivity between Kv1.2 and Kv1.3 [48]. Closer examination of this region reveals differences between Kv1.2- and Kv1.3-specific toxins in the number of residues with basic and acidic side chains (Table 3). Toxins with higher affinity for Kv1.3 tend to have a higher net charge in general, but more importantly, a higher net charge of the C-terminal half correlates well with higher selectivity for Kv1.3 over Kv1.2. Css20 fits this pattern

having only three basic residues (the dyad and two other lysines) in the C-terminal segment and higher affinity for Kv1.2. Furthermore, docking of Css20 to hKv1.2 and hKv1.3 predicts one hydrogen bond and several hydrophobic contacts of these non-dyad lysines (K33 and K35) with hKv1.2, but none with hKv1.3 (Fig. 6 and data not shown).

In addition, the residue two positions downstream of the critical lysine (framed in Table 3), which must be very close to the channel surface considering the protrusion of the lysine side chain into the selectivity filter, is an isoleucine in the high affinity Kv1.2 blockers, while it is a methionine in the Kv1.3-specific toxins. This isoleucine was identified as a key residue in the interaction of both CoTx1 [44] and Pi4 [45] with Kv1.2. The residue at the equivalent position in Css20 is an isoleucine (I30) matching the pattern of toxins selective for Kv1.2, and our docking results confirm that this residue is indeed closer to the bottom of the vestibule of hKv1.2 (ca. 2 Å) than that of hKv1.3 (ca. 5 Å) resulting in better contacts.

The N-terminal segments of the toxins containing the α-helical regions show no such obvious differences that could account for preferential binding to either of the channels, but the MTX-HsTx1 chimera experiments clearly demonstrate the crucial role of this region in binding as well. The replacement of the N-terminal half of HsTx1 with that of MTX reduced the affinity of the toxin for Kv1.3 almost 400-fold [48]. Three residues in this region of OSK1 were changed for residues found in kaliotoxin (OSK1-12, 16, 20, mutated residues underlined in Table 3), a highly selective blocker of Kv1.3, which resulted in an almost 10-fold increased selectivity for Kv1.3 [47]. The mutation K20D in OSK-1 alone resulted in an almost sevenfold improvement in Kv1.3 selectivity, and the equivalent residue, R14 in CoTx1 was found to interact with Kv1.2, suggesting that a basic residue at this position favors binding to Kv1.2 over Kv1.3 [44]. R19 of Pi4 is also an influential residue in binding to Kv1.2 and toxins specific for this channel bear an arginine or a glutamine at this position while toxins with lower affinity for Kv1.2 have uncharged or acidic residues with shorter side chains [45]. In this respect Css20 differs from the high affinity Kv1.2 blocking toxins having two alanines at

interacts with both channels at the selectivity filter, reason why these residues (Gly, Tyr) are not specifically indicated. Yellow outline box and arrows (middle panel) indicate α-helical and β-sheet structures of the toxin, respectively.

Table 3 – Sequence alignment and selectivity of toxins for Kv1.2- and Kv1.3-channels

	name	Peptide 123456789012345678901234567890	charge/His total	charge/His C-term	K$_d$ ratio Kv1.2/Kv1.3	K$_d$ (nM) Kv1.2	K$_d$ (nM) Kv1.3
Kv1.2	maurotoxin	VSCTGSKDCYAPCRKQTGCPNA-KCINKSCKCYGC	5/0	3/0	2e-4	0.7[a]	3300[a]
	CoTX1	AVCVYRT-CDKDCKRRGYRSG-KCINNACKCYPY	6/0	3/0	0.005	27[b]	5300[b]
	Pi4	IEAIRCGGSRDCYRPCQKRTGCPNA-KCINKTCKCYGCS	6/0	3/0	<8e-7	0.008[c]	>10000[c]
	Pi1	LVKCRGTSDCGRPCQQQTGCPNS-KCINRMCKCYGC	5/0	3/0	0.09	1[d]	11[e]
intermediate	Css20-3	IFINVKCSSPQQCLKPCKAAFGISAGGKCINGKCKCYP	6/0	3/0	0.2	1.5	7.2
	Noxiustoxin	TIINVKCTSPKQCSKPCKELYGSSAGAKCMNGKCKCYNN	6/0	3/0	2	2[f]	1[f]
	Hongotoxin-1	TVIDVKCTSPKQCLPPCKAQFGIRAGAKCMNGKCKCYPH	6/1	4/1	1.9	0.17[g]	0.09[g]
	ChTX	EFTNVSCTTSKECWSVCQRLHNTSRG-KCMNKKCRCYS	5/1	5/1	5.4	14[f]	2.6[f]
Kv1.3	anuroctoxin	ZKECTGPQHCTNFCRKNE-KCTHG-KCMNRKCKCFNCK	7/2	6/1	9	6[h]	0.7[h]
	OSK1	GVIINVKCKISRQCLEPCKKA-GMRFG-KCMNGKCHCTPK	8/1	4/1	386	5.4[i]	0.014[i]
	OSK1-20	GVIINVKCKISRQCLEPCKDA-GMRFG-KCMNGKCHCTPK	6/1	4/1	2108	78[i]	0.037[i]
	OSK1-12,16,20	GVIINVKCKISPQCLKPCKDA-GMRFG-KCMNGKCHCTPK	7/1	4/1	3322	196[i]	0.059[i]
	HsTX1	ASCRTPKDCADPCRKETGCPYG-KCMNRKCKCNRC	6/0	5/0	>45000	>500[j]	0.011[j]
	KTX	GVEINVKCSGSPQCLKPCKDAE-GMRFG-KCMNRKCHCTPK	6/1	5/1	>1538	>1000[f]	0.65[f]

dyad

Toxins are classified as Kv1.2 selective, intermediate and Kv1.3 selective based on the ratio of the dissociation constants for these channels. Next to the sequences the net charge and the number of histidine residues for the whole toxin are shown, then the same data for only the C-terminal segment of the toxin. The C- and N-terminal segments are separated by the dashed line. The residues of the "essential dyad" are indicated at the bottom. Residues likely to be important in determining selectivity for Kv1.2 or Kv1.3 are framed.
[a] hKv1.2 and hKv1.3 in COS-7 cells [43].
[b] rKv1.2 and mKv1.3 in mammalian cell lines [44].
[c] rKv1.2 and rKv1.3 in *Xenopus* oocytes [45].
[d] rKv1.2 in *Xenopus* oocytes [42].
[e] hKv1.3 in lymphocytes [46].
[f] rKv1.2 and mKv1.3 in mammalian cell lines [15].
[g] Kv1.2- and Kv1.3-channels in HEK-293 cells, Rb⁺-flux [29].
[h] hKv1.3 in lymphocytes and hKv1.2 in COS-7 cells [13].
[i] hKv1.2 in COS-7 cells and mKv1.3 in L929 or MEL cells [47].
[j] rKv1.2 in B82 and mKv1.3 in MEL cells [48].

the equivalent positions (residues 19 and 20). Other residues at the N-terminal region of Css20 are predicted to interact specifically with non-conserved residues at the turret, amongst these: S9 makes several contacts with the channel's residue at position Q357A for hKv1.2 and G375A for hKv1.3 whereas residue K18 of the toxin binds with residues in position E355 of subunit D of the hKv1.2, and T373 of subunit D of hKv1.3. Based on the criteria above, the low net charge of the C-terminal region, the presence of the dyad tyrosine (Y37), and the isoleucine at position 30 predict the higher affinity of Css20 for Kv1.2, whereas the alanines at positions 19 and 20 (alongside with the analogous interacting pairs between other toxin's N-terminal and channels' turret residues) probably work against it, resulting in a moderate selectivity for Kv1.2 over Kv1.3.

Both the development of steady-state block by Css20 and recovery from block were complete in 30 s for Kv1.3, while block development was about 10-times slower and recovery at least 30-times slower for Kv1.2. The striking differences in the rates of toxin association and dissociation to Kv1.2 and Kv1.3 indicate dissimilar modes of interaction with these channels in spite of the similar affinities. The fast association rate to Kv1.3 implies fast orientation at the early steps of docking, probably via through-space electrostatic interactions, but a number of unfavorable close contact interactions are likely to be the reason for the equally fast dissociation [49]. Docking results are in complete agreement with this scenario; most of the interacting residues of hKv1.3 are those of the selectivity filter, which make contacts mainly with the toxin's plugging residue K28. On the other hand, toxin orientation during docking to Kv1.2 seems less aided by through-space electrostatics, but the contact surface of Css20 better suits Kv1.2, with an extensive hydrogen bonding network – as predicted by the docking – between channel's turret residues and axially located residues of the toxins, leading to slower dissociation and an overall higher affinity.

4.1. Scope and limitations of molecular docking

Docking algorithms have experienced a considerable improvement in the last few years, to the point that exhaustive searching of interaction modes between targets of known structure usually predicts at least one right solution amongst the 100 best scoring predictions; however, discrimination across different solutions is usually achieved by scoring functions (here, we have used ZRANK and FireDock), all of which still have limited performance [50]. In our case, we have discarded Css20 interaction with hKv1.1 and hKv1.4 on the basis of combined poor docking parameters (see Table 2); however, the best solution for docking to hKv1.1 was not

significantly different from docking to hKv1.2 and hKv1.3 (not shown). The level of "discrimination" we have attained clearly benefited from the concomitant analysis of several closely related predictions. Our docking approach could be considered inappropriate, because we have extracted a single interaction mode (which we have called "principal mode") amongst several other docking candidates. However, this selection was based on compiling evidence regarding the interaction mode of subfamily 2 α-Ktxs and Kv1-channels [35,36]. Our rationale relies on the fact that K28 of the toxin should interact with the selectivity filter as "plug-in"; hence while extracting the docking solutions in which this interaction was conserved, we were restraining the binding modes to those which are in agreement with this, experimentally determined, homologous interacting pair. Nonetheless, it is worthy to remember that any molecular model is always speculative. As stated above, we are taking advantage of compelling evidence regarding this particular interacting pair, which provides us with a reasonable hypothesis regarding why and how Css20 discriminates Kv1.2 and Kv1.3 over other channels, and the differences between mechanistically similar binding to Kv1.2- and Kv1.3-channels. Obviously, in the absence of such compelling evidence, the models by themselves would be of poor help if any.

5.   Concluding remarks

Several scorpion toxins have been purified so far that have similar affinities for Kv1.2 and Kv1.3-channels, such as Css20, the subject of this study. The observations from sequence comparisons, mutant cycle analyses and models of toxin docking can enable us to improve toxin selectivity for either of the channels. For instance, disrupting Kv1.2-specific interactions of Css20 (Q11 and K33 with E355 in different subunits), could increase Kv1.3 selectivity. Such an approach, successful for other scorpion toxins [51], would allow targeting appropriate cells and physiological/pathophysiological functions. Further studies are required to explore this scenario, which can be guided by the analysis presented in this study.

Acknowledgements

REFERENCES

[1] Panyi G, Possani LD, Rodríguez de la Vega RC, Gáspár R, Varga Z. K+ channel blockers: novel tools to inhibit T cell activation leading to specific immunosuppression. Curr Pharm Des 2006;12:2199–220.

[2] Panyi G, Varga Z, Gaspar R. Ion channels and lymphocyte activation. Immunol Lett 2004;92:55–6.

[3] Leonard RJ, Garcia ML, Slaughter RS, Reuben JP. Selective blockers of voltage-gated K+ channels depolarize human T lymphocytes: mechanism of the antiproliferative effect of charybdotoxin. Proc Natl Acad Sci USA 1992;89: 10094–8.

[4] Kalman K, Pennington MW, Lanigan MD, Nguyen A, Rauer H, Mahnir V, et al. ShK-Dap22, a potent Kv1.3-specific immunosuppressive polypeptide. J Biol Chem 1998;273:32697–707.

[5] Wulff H, Beeton C, Chandy KG. Potassium channels as therapeutic targets for autoimmune disorders. Curr Opin Drug Discov Dev 2003;6:640–7.

[6] Rauer H, Lanigan MD, Pennington MW, Aiyar J, Ghanshani S, Cahalan MD, et al. Structure-guided transformation of charybdotoxin yields an analog that selectively targets Ca(2+)-activated over voltage-gated K(+) channels. J Biol Chem 2000;275:1201–18.

[7] Coleman SK, Newcombe J, Pryke J, Dolly JO. Subunit composition of Kv1 channels in human CNS. J Neurochem 1999;73:849–58.

[8] Dodson PD, Billups B, Rusznák Z, Szûcs G, Barker MC, Forsythe ID. Presynaptic rat Kv1.2 channels suppress synaptic terminal hyperexcitability following action potential invasion. J Physiol 2003;550:27–33.

[9] Rasband MN, Park EW, Vanderah TW, Lai J, Porreca F, Trimmer JS. Distinct potassium channels on pain-sensing neurons. Proc Natl Acad Sci USA 2001;98:13373–8.

[10] Valdez-Cruz NA, Batista CV, Possani LD. Phaiodactylipin, a glycosylated heterodimeric phospholipase A from the venom of the scorpion *Anuroctonus phaiodactylus*. Eur J Biochem 2004;271:1453–64.

[11] Batista CV, Del Pozo L, Zamudio FZ, Contreras S, Becerril B, Wanke E, et al. Proteomics of the venom from the Amazonian scorpion *Tityus cambridgei* and the role of prolines on mass spectrometry analysis of toxins. J Chromatogr B Anal Technol Biomed Life Sci 2004;803:55–66.

[12] Corzo G, Adachi-Akahane S, Nagao T, Kusui Y, Nakajima T. Novel peptides from assassin bugs (Hemiptera: Reduviidae): isolation, chemical and biological characterization. FEBS Lett 2001;499:256–61.

[13] Bagdany M, Batista CV, Valdez-Cruz NA, Somodi S, Rodriguez de la Vega RC, Licea AF, et al. Anuroctoxin, a new scorpion toxin of the alpha-KTx 6 subfamily, is highly selective for Kv1.3 over IKCa1 ion channels of human T lymphocytes. Mol Pharmacol 2005;67:1034–44.

[14] Deutsch C, Krause D, Lee SC. Voltage-gated potassium conductance in human T lymphocytes stimulated with phorbol ester. J Physiol 1986;372:405–23.

[15] Grissmer S, Nguyen AN, Aiyar J, Hanson DC, Mather RJ, Gutman GA, et al. Pharmacological characterization of five cloned voltage-gated K+ channels, types Kv1.1, 1.2, 1.3, 1.5, and 3.1, stably expressed in mammalian cell lines. Mol Pharmacol 1994;45:1227–34.

[16] Avdonin V, Tang XD, Hoshi T. Stimulatory action of internal protons on Slo1 BK channels. Biophys J 2003;84:2969–80.

[17] Berman HM, Westbrook J, Feng Z, Gilliland G, Bhat TN, Weissig H, et al. The Protein Data Bank. Nucleic Acids Res 2000;28:235–42.

[18] Altschul SF, Madden TL, Schäffer AA, Zhang J, Zhang Z, Miller W, et al. Gapped BLAST and PSI-BLAST: a new generation of protein database search programs. Nucleic Acids Res 1997;25:3389–402.

[19] Eswar N, Marti-Renom MA, Webb B, Madhusudhan MS, Eramian D, Shen MY, et al. Comparative protein structure

modeling using modeller, vol. 15. New York: John Wiley & Sons, Inc.; 2006.

[20] Azuara C, Lindahl E, Koehl P, Orland H, Delarue M. PDB_Hydro: incorporating dipolar solvents with variable density in the Poisson–Boltzmann treatment of macromolecule electrostatics. Nucleic Acids Res 2006;34:W38–42.

[21] Chen R, Li L, Weng Z. ZDOCK: an initial-stage protein-docking algorithm. Proteins 2003;52:80–7.

[22] Pierce B, Weng Z. ZRANK: reranking protein docking predictions with an optimized energy function. Proteins 2007;67:1078–86.

[23] Pettersen EF, Goddard TD, Huang CC, Couch GS, Greenblatt DM, Meng EC, et al. UCSF Chimera—a visualization system for exploratory research and analysis. J Comput Chem 2004;25:1605–12.

[24] Andrusier N, Nussinov R, Wolfson HJ. FireDock: fast interaction refinement in molecular docking. Proteins 2007;69:139–59.

[25] Krissinel E, Henrick K. Inference of macromolecular assemblies from crystalline state. J Mol Biol 2007;372: 774–97.

[26] Koradi R, Billeter M, Wüthrich K. MOLMOL: a program for display and analysis of macromolecular structures. J Mol Graph 1996;14:51–5.

[27] Wallace AC, Laskowski RA, Thornton JM. LIGPLOT: a program to generate schematic diagrams of protein–ligand interactions. Protein Eng 1995;8:127–34.

[28] Tytgat J, Chandy KG, Garcia ML, Gutman GA, Martin-Eauclaire MF, van der Walt JJ, et al. A unified nomenclature for short-chain peptides isolated from scorpion venoms: alpha-KTx molecular subfamilies. Trends Pharmacol Sci 1999;20:444–7.

[29] Koschak A, Bugianesi RM, Mitterdorfer J, Kaczorowski GJ, Garcia ML, Knaus HG. Subunit composition of brain voltage-gated potassium channels determined by hongotoxin-1, a novel peptide derived from Centruroides limbatus venom. J Biol Chem 1998;273:2639–44.

[30] Shen W, Hernandez-Lopez S, Tkatch T, Held JE, Surmeier DJ. Kv1.2-containing K$^+$ channels regulate subthreshold excitability of striatal medium spiny neurons. J Neurophysiol 2004;91:1337–49.

[31] Garcia-Calvo M, Leonard RJ, Novick J, Stevens SP, Schmalhofer W, Kaczorowski GJ, et al. Purification, characterization, and biosynthesis of margatoxin, a component of Centruroides margaritatus venom that selectively inhibits voltage-dependent potassium channels. J Biol Chem 1993;268:18866–74.

[32] Olamendi-Portugal T, Somodi S, Fernández JA, Zamudio F, Becerril B, Varga Z, et al. Five novel alfa-KTx peptides from the venom of the scorpion Centruroides elegans selectively block Kv1.3 over IKCa1 K$^+$ channels of T cells. Toxicon 2005;46:418–29.

[33] Peter MJ, Varga Z, Hajdu P, Gaspar RJ, Damjanovich S, Horjales E, et al. Effects of toxins Pi2 and Pi3 on human T lymphocyte Kv1.3 channels: the role of Glu7 and Lys24. J Membr Biol 2001;179:13–25.

[34] Miller C. The charybdotoxin family of K$^+$-channel-blocking peptides. Neuron 1995;15:5–10.

[35] Rodriguez de la Vega RC, Merino E, Becerril B, Possani LD. Novel interactions between K$^+$ channels and scorpion toxins. Trends Pharmacol Sci 2003;24:222–7.

[36] Giangiacomo KM, Ceralde Y, Mullmann TJ. Molecular basis of alpha-KTx specificity. Toxicon 2004;43:877–86.

[37] Yi H, Cao Z, Yin S, Dai C, Wu Y, Li W. Interaction simulation of hERG K$^+$ channel with its specific BeKm-1 peptide: insights into the selectivity of molecular recognition. J Proteome Res 2007;6:611–20.

[38] Yi H, Qiu S, Cao Z, Wu Y, Li W. Molecular basis of inhibitory peptide maurotoxin recognizing Kv1.2 channel explored by ZDOCK and molecular dynamic simulations. Proteins 2008;70:844–54.

[39] Isacoff EY, Jan YN, Jan LY. Evidence for the formation of heteromultimeric potassium channels in Xenopus oocytes. Nature 1990;345:530–4.

[40] Bednarek MA, Bugianesi RM, Leonard RJ, Felix JP. Chemical synthesis and structure–function studies of margatoxin, a potent inhibitor of voltage-dependent potassium channel in human T lymphocytes. Biochem Biophys Res Commun 1994;198:619–25.

[41] Dauplais M, Lecoq A, Song J, Cotton J, Jamin N, Gilquin B, et al. On the convergent evolution of animal toxins. Conservation of a diad of functional residues in potassium channel-blocking toxins with unrelated structures. J Biol Chem 1997;272:4302–9.

[42] Mouhat S, Mosbah A, Visan V. The 'functional' dyad of scorpion toxin Pi1 is not itself a prerequisite for toxin binding to the voltage-gated Kv1.2 potassium channels. Biochem J 2004;377:25–36.

[43] Visan V, Fajloun Z, Sabatier JM, Grissmer S. Mapping of maurotoxin binding sites on hKv1.2, hKv1.3, and hIKCa1 channels. Mol Pharmacol 2004;66:1103–12.

[44] Jouirou B, Mosbah A, Visan V, Grissmer S, M'Barek S, Fajloun Z, et al. Cobatoxin 1 from Centruroides noxius scorpion venom: chemical synthesis, three-dimensional structure in solution, pharmacology and docking on K$^+$ channels. Biochem J 2004;377:37–49.

[45] M'Barek S, Mosbah A, Sandoz G, Sabatier JM. Synthesis and characterization of Pi4, a scorpion toxin from Pandinus imperator that acts on K$^+$ channels. Eur J Biochem 2003;270:3583–92.

[46] Péter MJ, Hajdu P, Varga Z, Damjanovich S, Possani LD, Panyi G, et al. Blockage of human T lymphocyte Kv1.3 channels by Pi1, a novel class of scorpion toxin. Biochem Biophys Res Commun 2000;278:34–7.

[47] Mouhat S, Visan V, Ananthakrishnan S, Andreotti HN, Darbon H, De Waard M, et al. K$^+$ channel types targeted by synthetic OSK1, a toxin from Orthochirus scrobiculosus scorpion venom. Biochem J 2005;385:95–104.

[48] Regaya I, Beeton C, Ferrat G, Andreotti N, Darbon H, De Waard M, et al. Evidence for domain-specific recognition of SK and Kv channels by MTX and HsTx1 scorpion toxins. J Biol Chem 2004;279:55690–6.

[49] Goldstein SA, Pheasant DJ, Miller C. The charybdotoxin receptor of a Shaker K$^+$ channel: peptide and channel residues mediating molecular recognition. Neuron 1994;12:1377–88.

[50] Lensink MF, Méndez R, Wodak SJ. Docking and scoring protein complexes: CAPRI 3rd Edition. Proteins 2007;69: 704–18.

[51] Mouhat S, Teodorescu G, Homerick D, Visan V, Wulff H, Wu Y, et al. Pharmacological profiling of Orthochirus scrobiculosus toxin 1 analogs with a trimmed N-terminal domain. Mol Pharmacol 2006;69:354–62.